Three-Dimensional Seismic Endoscopy—Part I: Design of Apparatus and Basic Imaging Algorithms

Henri-Pierre Valero, Ginette Saracco, and Dominique Gibert

Abstract—A method, called "seismic endoscopy," able to per-form three-dimensional (3-D) acoustical imaging in a cylindrical volume around shallow-depth boreholes is described. The main characteristics of borehole tools designed and constructed in our laboratory are presented. Several tests performed in an acoustical water tank are used to illustrate the basic imaging algorithms adapted to the particular acquisition geometry of the probes. In particular, both the filtering of borehole waves and azimutal refocusing are discussed.

Index Terms—Azimuthal move out (AMO), borehole waves, continuous wavelet transform, three-dimensional (3-D) geophys-ical imaging, tube waves, vertical seismic profile.

I. Introduction

HIGH-RESOLUTION geophysical imaging of the subsurface is increasingly used in civil or reservoir engineering [1], environmental studies [2], [3], and hydrogeology [4], [5]. Applications, for instance, concern geotechnical investigations prior to building construction, tunnels monitoring, chemical and nuclear waste disposals, and water resource evaluation. Difficulties commonly encountered when performing geophysical experiments in these types of applications are the short time periods available to perform the field measurements, the poor accessibility of the earth's surface especially in urban areas, and the noisy (both electromagnetic and seismic) environment in which the measurements are made [6], [7]. Also, low-diameter ($\leq$6 cm) and shallow-depth ($\leq$30 m) geotechnical boreholes are often available for various geophysical techniques. In this context, we recently engaged in studies concerning the design of a borehole apparatus able to acquire directional data and to produce three-dimensional (3-D) seismic images in a cylindrical volume surrounding the concerned borehole. This imaging should concern a cylinder with a radius of several meters.

The advantage of this methodology in comparison to the others lies in the addition of a directional azimuthal parameter θ. The acquisition of conventional sonic [8] frequency range of the source around 1–20 kHz, or VSP [9], [10] frequency between 80 and 100 Hz is defined by only three parameters: the distance between the transmitter and the receivers, i.e., the offset ζ, the depth of the transmitter z, and the time t related to the recorded waveforms. The scale of investigation is just different. Nevertheless, the azimuthal information can be introduced using a multicomponents VSP acquisition, but not in a direct way. This requires downloading a large collection of data, and the azimuthal information is obtained after a process by merging the recorded data along the three axis. The only tool that performs a direct azimuthal acquisition is the televiewer [14], which is composed of a directional transducer, which allows measurement at very high frequencies (around 500 MHz), the normal reflected field of the borehole wall. However, owing to the frequency range used, it is not possible to perform an image beyond the wall.

In the present method, the directive azimuthal information is obtained directly during the acquisition using a single cell of sensors without any kind of processing. The frequency range of the source signal is around 40–120 kHz. We acquire data depending on four degrees of freedom (DOF) (θ, t, z, ζ) with respect to the cylindrical geometry of the borehole acquisition. We will call *cylinder of data* a collection of data depending on the four parameters.

In this paper, we present the first results concerning the design and construction of a prototype of directional probe. A preprocessing algorithm suitable for the particular acquisition geometry pertaining to this kind of apparatus is also discussed. In Section II, we describe the experimental setup and show water tank experiments to illustrate the basic concepts of the method. A basic imaging algorithm taking into account the cylindrical geometry of the data acquisition is presented in Section III. This allows us to focus the data in the azimuthal domain. Some tests on synthetic and noisy data show its efficiency. The application of azimuthal move out (AMO) algorithm on experimental data is analyzed in Section IV. First, we prove the azimuthal refocusing of seismic sections recorded in a water tank in the presence of different scatterers located at different directions and distances for the probe. Second, we filter the borehole waves generated by a concrete miniature pipe introduced in the tank without scatterers around. In a third experimental application, described in Section V, a metallic object is placed outside a real concrete pipe. This presents a defectiveness with a response in the same frequency range as the target. An initial post-processing combining wavelet technique and azimuthal algorithm to filter borehole modes and localize this object in the plane (θ, t), when z

This work was initially supported by the CNRS-INSU GdR "Géomécanique des Roches Profondes" and is now supported by the CNRS and ANDRA through the GdR FORPRO (Research Action 99-II) and corresponds to the GDR FORPRO Con-tribution 2000/02 A.

H.-P. Valero was with IPG, Paris, France, and Géosciences Rennes (CNRS-UPR 4661), UER I, F-35042 Rennes Cedex, France. He is now with Schlumberger K.K., Sonic Interpretation Product Line, Kanagawa-ken 229-0006, Japan (e-mail: valero@fuchinobe.skk.slb.com).

G. Saracco and D. Gibert are with Géosciences Rennes (CNRS-UPR 4661), UER I, F-35042 Renne Cedex, France (e-mail: ginet@univ-rennes1.fr; gibert@univ-rennes1.fr).

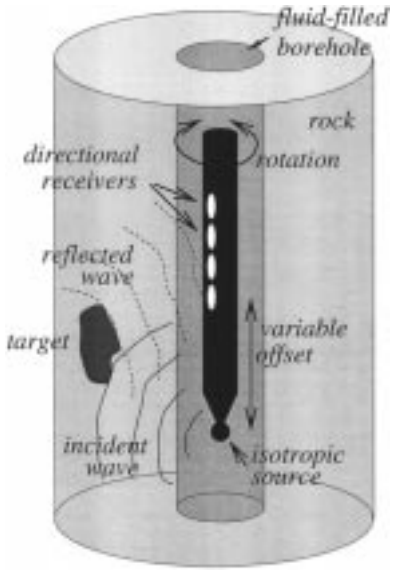

Fig. 1. Principle of the 3-D seismic endoscopy. A probe equipped with an acoustical source records azimuthally, from directive receivers, the echoes coming from targets located around the borehole.

and ζ are constant, is presented. Section VI is devoted to conclusions. The sensitivity of the AMO algorithm is discussed in the Appendix.

II. Experimental Setup

A. Principle of Method and Operating Constraints

The new points of this method include the introduction of the azimuthal information during the data acquisition controlled by a specific antenna of directive receivers that we call "ear," by analogy with the human ear. This receiver cell plays the same role to detect and discriminate a specific sound or echoes submerged in a surrounding noise. This allows us to perform a 3-D acoustical imaging in a cylindrical volume around the borehole. Azimuthal information is related to the rotation of the tool inside the borehole, while directive acquisition is defined by the cone of influence (or aperture) of the ear, with respect to the wavelength of the source signal.

The principle of the method is shown in Fig. 1. The probe is equipped with both a controlled source and an antenna of directive receivers.

At each depth stage, the source is fired while the probe rotates and records the echoes reflected by the heterogeneities located in the vicinity of the borehole [15]. From the point of view of conventional surface seismic processing, the depth z of the source of the probe is equivalent to the along-roll position of the surface seismic source.

As in seismic surface acquisition, the offset ζ between the source and the receivers is an important DOF that can be used to make the velocity analysis prior to stacking while its range (or aperture) controls the focusing performances of migration techniques.

The azimuth θ is a new acquisition parameter with no direct equivalent in standard surface seismics. The azimuthal resolution of the antenna depends both on the diameter of the probe and on the frequency range of the source signals. The properties of the surrounding rock medium does not play an important role in the directivity properties of the tool, but in the penetrating power of the source signal with different effects of scattering, diffusion, or/and attenuation and absorption. This implies a variation of the form of the volumic data acquisition (deformed cylinder). The localization in time and space of scatterers will be conserved, but not the amplitude of the scattered field. If we want to analyze 6–10 m around the probe with a spatial resolution of few centimeters and an azimuthal precision of 10°, it is necessary with a realistic diameter of the probe of 6 or 8 cm, to have a frequency range of the source between 20 kHz and 200 kHz. The diameter of the probe was fixed to 6 cm (see Fig. 2) to perform field experiments in standard geotechnical boreholes while the source frequency range (40 kHz–120 kHz) allows us to acquire both experiments in the acoustic tank and small-scale field studies. Lower frequencies should be used in future to image areas far from the borehole.

Fig. 2. Prototype of directional probe during an experiment in the water tank. The isotropic source is located in the wider part at the very bottom of the probe. Directly above it is the window in the absorbing material containing the receivers. The stepping motor visible at the top of the figure controls the rotation of the whole probe.

The global structure of data acquisition presented earlier offers four DOF which allows different ways to analyze the data depending of some specificities of the problem. Let $C(\theta, t, z, \zeta)$ be the function describing the recorded cylinder of data.

If θ is constant ($\theta = \theta_o$), we obtain as expected the standard two-dimensional (2-D) seismic section in the plane (z, t). In

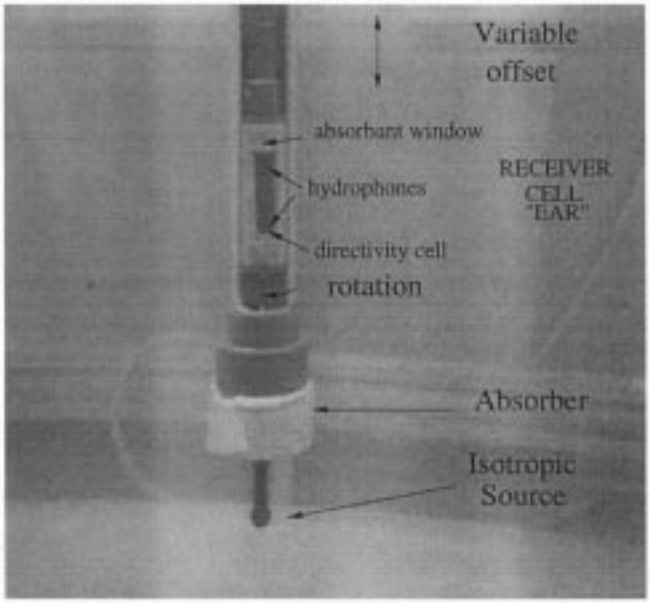

Fig. 3. Window of directivity including the receiver cell (pair of hydrophones) embedded in the absorbing material, called "ear."

this case, we can apply the processing used for current borehole seismic (see [16], [17]).

For a constant depth $z = z_o$, we get a 2-D tomographic section in the plane (θ, t) depending on the parameter ζ. The analysis of data is based on the maximum time. However, the variable t plays the same role as the radius r of the cylinder of data, respectively, to the penetrating power of the wave. This can be useful to quickly detect some objects around the borehole versus azimuth. The assumption made in this case is that the waves propagate only in the plane (θ, t). The *cylinder of data* can be analyzed with different parameters combinations, which allow us to play independently on each one.

B. Probe Characteristics

The azimuthal directivity can be obtained in several ways. We have chosen to use omnidirectional hydrophones (source and receivers), and to limit the recording in a close angular sector. The choice of the aperture depends on the working frequency, and the spatial resolution to which it is aimed. A cylinder of absorbing material with a narrow window where the piezoelectric transducers are embedded is used to define the angular sector (Fig. 3). The "ear" aperture was designed to have a width of 3 cm in the horizontal axis and 7 cm in the vertical axis.

This solution has the advantage of being easily adjustable at a low cost, because changing the directional characteristics only involves reshaping another cylinder of absorbing material while keeping the same piezoelectric transducers. Nevertheless, decreasing the ear aperture, to obtain a good directivity, will be done by considering also the signal-to-noise ratio (SNR) expected on the recorded data. These physical conditions will be closely related to the wavelength that we will measure.

The offset may be varied by using either a static antenna with numerous receivers or a mobile one with a small number of receivers. We adopted the latter solution, i.e., a cell with two receivers (Fig. 3). The offset of the antenna is controlled through an aluminum rod emerging at the top of the borehole.

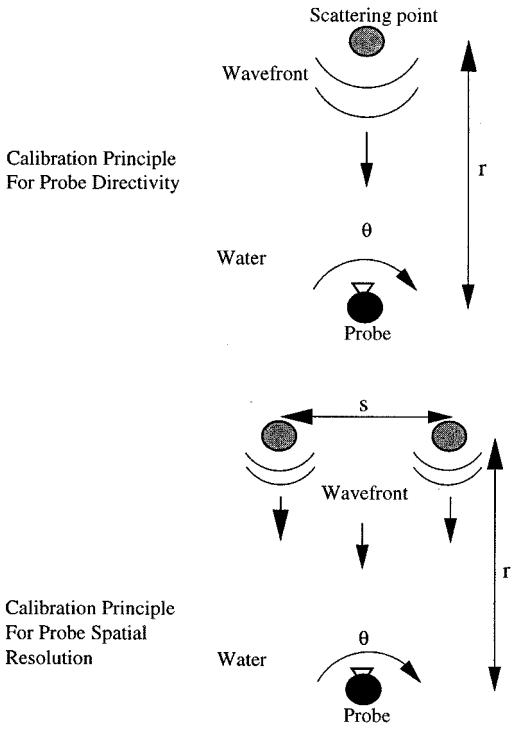

Fig. 4. Calibration protocol experiment performed to obtain the azimuthal directivity and spatial resolution of the probe.

This technological solution limits to about 10 m the maximum depth at which the probe can operate. Greater depths could be reached by replacing the rod controlling the offset with a remotely controlled jack, with respect to the problem of the increasing pressure at very high depth. The prototype used in this study has an offset range given by 15 cm $\leq \zeta \leq$ 80 cm. The antenna will detect the maximum amount of energy coming from heterogeneities located around 1 m away from the probe. In field experiments where the targets are more distant, the offset range should be increased to conserve the same ratio of energy. The offset increment must be small enough to prevent spatial aligning of the incoming acoustical waves reflected by the surrounding targets ($\delta\zeta \simeq 1$ cm, in the present study).

The azimuthal directivity and spatial resolution of the directional cell, i.e., "ear," need to be quantified to evaluate the resolution and limitation of the probe. Because it is not possible to evaluate in real conditions the spatial resolution and azimuthal directivity of the probe, we decided to calibrate the tool in a reference medium (water). The tool properties obtained will be related to the wavelength of the signal, i.e., the velocity of the medium where the signal will propagate. Knowing the directivity and the spatial resolution of the tool in a reference medium, it is then possible to predict the behavior of the tool, which will be helpful to interpret the measurement in real condition. This assumption is usually done in georadar technology where the directivity of the antenna is known only in the reference medium and not for real acquisition conditions. In our case it was not possible to make this calibration with fluid-like mud commonly used in borehole logging. We have some technical limitations to perform acoustic laboratory experiments. This explains the choice of the water as reference medium.

Fig. 4 presents the protocol developed to calibrate the probe [18] in the water acoustic tank. The azimuthal directivity is mea-

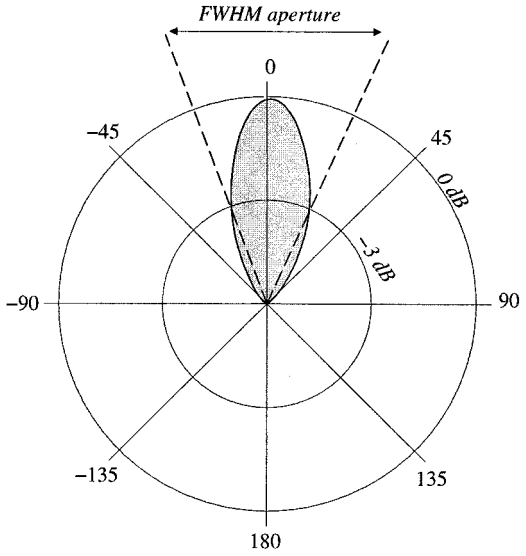

Fig. 5. Directivity pattern of the probe for the 50–70 kHz frequency range.

sured by firing a point source (small and omnidirectional piezoelectric) located at a distance r from the tool and at the same depth as the azimuthal receiver. For example, Fig. 5 shows the azimuthal directivity obtained at the distance $r = 90$ cm. The amplitude of the signal is drawn for discrete angles and for the frequency range of interest for real experiments. One can observe that the directivity is sharp, with a full-width half-maximum aperture of about $\alpha = 45°$.

The spatial resolution evaluation is obtained by conducting a similar experiment. Two omnidirectional piezoelectric sources separated by a distance s and located at a distance r from the probe are positioned in the acoustic tank at the same depth. The emission of these two signals is synchrone and controlled by a computer. The spatial resolution of the probe is evaluated for several distances s and r versus azimuth for different frequencies. Fig. 6 shows the result of this calibration. Two objects located at 50 cm from the probe and separated by 12 cm can be resolved. This is accurate enough regarding our objective, which is to detect surface and not just some single scattering points.

The prototype of the probe developed for this study, along with its physical properties, was presented in this section. The main limitation of this prototype is related to the fact that the electronic and power devices are located at the surface, which limits the depth of use of the tool. To manage this technical limitation, we designed the probe to be able to perform acquisition at a depth of 10 m from the surface. In this condition, the pressure and the temperature of the borehole are not a critical issue and are therefore not a problem for the current probe. For the next generation of probe, we will consider the possibility of putting electronics inside the tool to avoid these limitations. In the near future, we will consider changing the rotation of the tool with an electronic rotation of a specific (ring or ellipsoid) antenna, and improving the transfer of data by using optical fibers.

III. Azimuthal Move Out (AMO)

A. Principle of the Method

The aim of the AMO is to sharpen the angular resolution of the probe by correcting the transfer function of the receivers

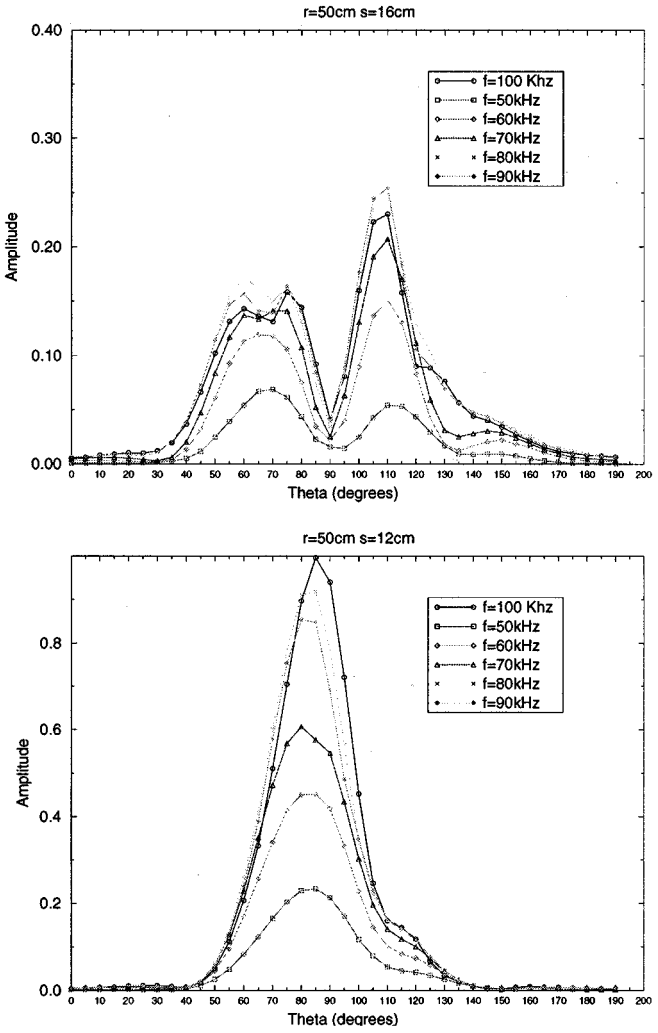

Fig. 6. Spatial resolution of the probe for different frequencies and different distances source-probe. We reach the limit of resolution when two points are separated by 12 cm when they are located at a distance of 50 cm from the probe.

[19]. The variation of the amplitude with respect to the azimuth, already shown in Fig. 5, is not the only property which can be used to make an angular correction. We found it more efficient to use a time delay property because the echoes coming from targets located in the limit of the visibility angle of the receiver arrive slightly later than echoes associated with targets located in front of the receiver. It follows that the acoustic response of a point-like target will be shared out like a set of hyperbolas centered around the azimuthal position of the target, presenting a flat apex. This set will be more or less dilated with respect to the distance target-receiver. Fig. 7 shows the response of a point-like source located 0.90 m from the probe in the azimuthal direction $\theta = 180°$. The arrival times of the signal are on a smooth curve whose flat apex is located in front of the point source. This particular shape can be understood by remembering that the directivity of the "ear" is obtained by embedding omnidirectional piezoelectric sensors into an open cylinder of absorbing material: assuming a high-frequency asymptotic regime, Fig. 8 shows how the rays connecting the diffracting source to the receivers are no more straight but slightly longer, whenever the source is not centered on the aperture of the absorbing cylinder

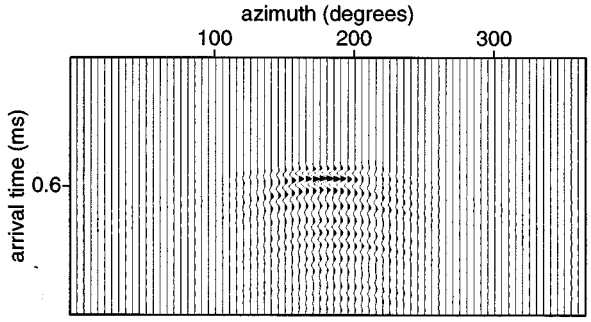

Fig. 7. Recorded signal of a point-like source located at $\theta = 180°$.

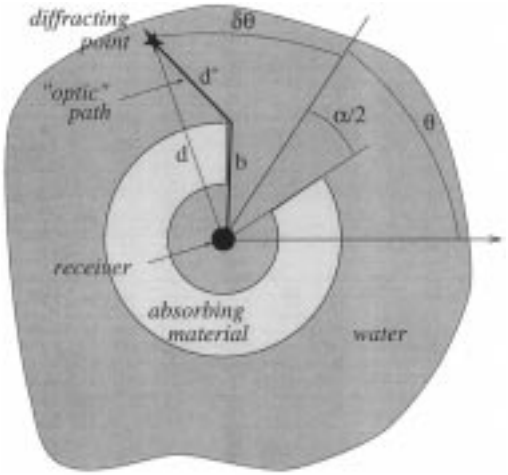

Fig. 8. Top view of the azimuthal receiver. The wave echoed by a target located outside the visibility angle $\theta \pm \alpha/2$ follows an "optic" path longer than the direct paths followed by the echoes coming from targets located in the visibility angle. This explains the time delays observed in the data shown in Fig. 7.

("ear"). This results in later arrival times in accordance with the different trajectories of rays. When $|\delta\theta| > \alpha/2$, the arrival time is given by

$$t(\delta\theta|\theta) = t_b + \sqrt{t_b^2 + t_0^2 - 2t_b t_0 \cos\left(|\delta\theta| - \frac{\alpha}{2}\right)} \qquad (1)$$

where

t_b $= b/c_w$;
t_0 $= d1/c_w$;
c_w sound velocity in water;
α aperture angle of the window opened in the absorbing cylinder and which will be referred to as the *visibility angle* in the remainder of this paper.

See Fig. 8 for definition of symbols. In geological situations, we have $t_b = b/c_m$ and $t_0 = d1/c_w$, where c_m is the sound velocity in the borehole mud and c_r is an AMO velocity which depends on the velocity in the surrounding rocks and corresponds to the mean velocity for which the AMO stacking is most efficient. In field situations, (1) can be completed to account for a possible distance between the probe axis and the center of the borehole. We can also introduce the "angular ray" parameter in (1), defined by

$$p = \frac{\left|\sin\left(|\theta| - \frac{\alpha}{2}\right)\right|}{c}.$$

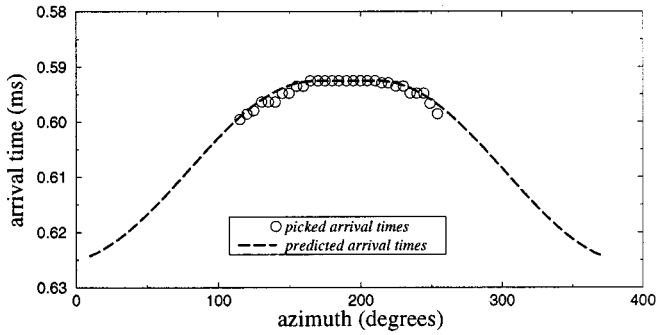

Fig. 9. Arrival times picked from the signal shown in Fig. 7 and times predicted by (1).

Fig. 9 shows the arrival times picked from the signal shown in Fig. 7, together with the times calculated by (1). Although (1) was obtained from a crude infinite-frequency approximation, it can be seen that the predicted arrival times accurately agree with the ones picked from the data. In particular, the flat apex is very well reproduced.

Equation (1) can be used to correct the bias in the arrival times outside the visibility angle by applying an azimuthal dynamic correction very similar to the classical normal move out (NMO) correction in seismics [20]. This correction is done by stacking all traces along curves whose arrival times are $t(\delta\theta|\theta)$ for both given θ and t_0. This stacking cancels the nonaligned echoes and enhances the aligned ones with an improvement of the SNR. In this procedure, random noise present in the data also partly cancels. The dynamic of the resultant stacked trace is enhanced by a weighting function. The best function in our case is the absolute value of the trace referenced by the azimuth θ. We present in the Appendix the sensitivity of the method.

B. Application to Synthetic Data

This section is devoted to the study of the AMO correction on synthetic examples with and without noise. As shown in Fig. 7, the amplitude response of one scattering point recorded by the probe is a function of the travel-time object-probe, and the azimuth. The travel time is calculated using the AMO equation, as previously shown in Fig. 9. The amplitude depends on the directivity of the probe, which is itself a function of the azimuth. We can notice that the directivity function can be approximated by a Gaussian curve which is consistent with the assumption made on a high-frequency asymptotic regime. The fitting between the directivity data and a Gaussian function is presented in Fig. 10. For this reason, the theoretical directivity is defined as

$$A(\theta, \alpha) = \exp\left(\frac{-\theta^2}{\left(\frac{\alpha}{2}\right)^2}\right) \qquad (2)$$

where α corresponds to the angular aperture of the ear that determines the directivity of the probe (Fig. 5).

The only restriction of this modeling is due to the fact that Gaussian functions do not exist on the circle, only functions with compact support. That is not the case of the directivity function. To avoid this theoretical problem, we consider that this function will be zero outside the range $[-\theta_c, \theta_c]$. θ_c corresponds to an

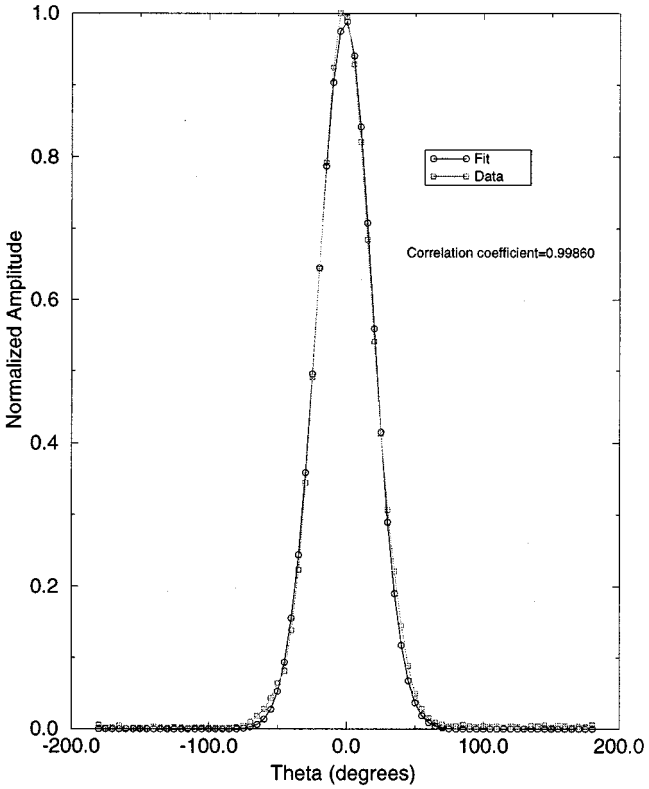

Fig. 10. Comparison between the directivity data and the fit obtained with a Gaussian function.

azimuthal cutoff defined from the directivity function presented above. This assumption is consistent with our experiments in acoustic laboratory, in so far as we can assume it to be valid. This directivity is computed in the absence of the borehole in a reference medium (water). In the presence of real borehole, this directivity function will change, but as with radar, we do not need a very accurate knowledge of the directivity; we just want to discriminate echoes coming far from the borehole. The knowledge of this function in reference medium will be useful to define the limitation of the directivity depending on the real conditions. An experiment in the presence of miniature concrete borehole (see Section IV) shows that the concept of directivity is also valid in the presence of the borehole.

The modeling of the different tests presented here was done using ray tracing theory. The first group of synthetic tests consists of building the response of one and two scattering points recorded by the probe. Fig. 11 show results after AMO correction. In both cases, we can nicely refocus the information, according to the vision angle of the probe. The second group of tests uses the same data set $s(t)$ with an additional white Gaussian noise and a signal-over-noise ratio sn equal to 2 [21]. This means that

$$\tilde{s}(t) = s(t) + \text{scale} * \text{noise}$$

with

$$\text{scale} = \left(\frac{1}{sn}\right) * \frac{\left(\frac{|\max(\text{signal})|}{\sqrt{2}}\right)}{\sqrt{\text{energy per sample}}}.$$

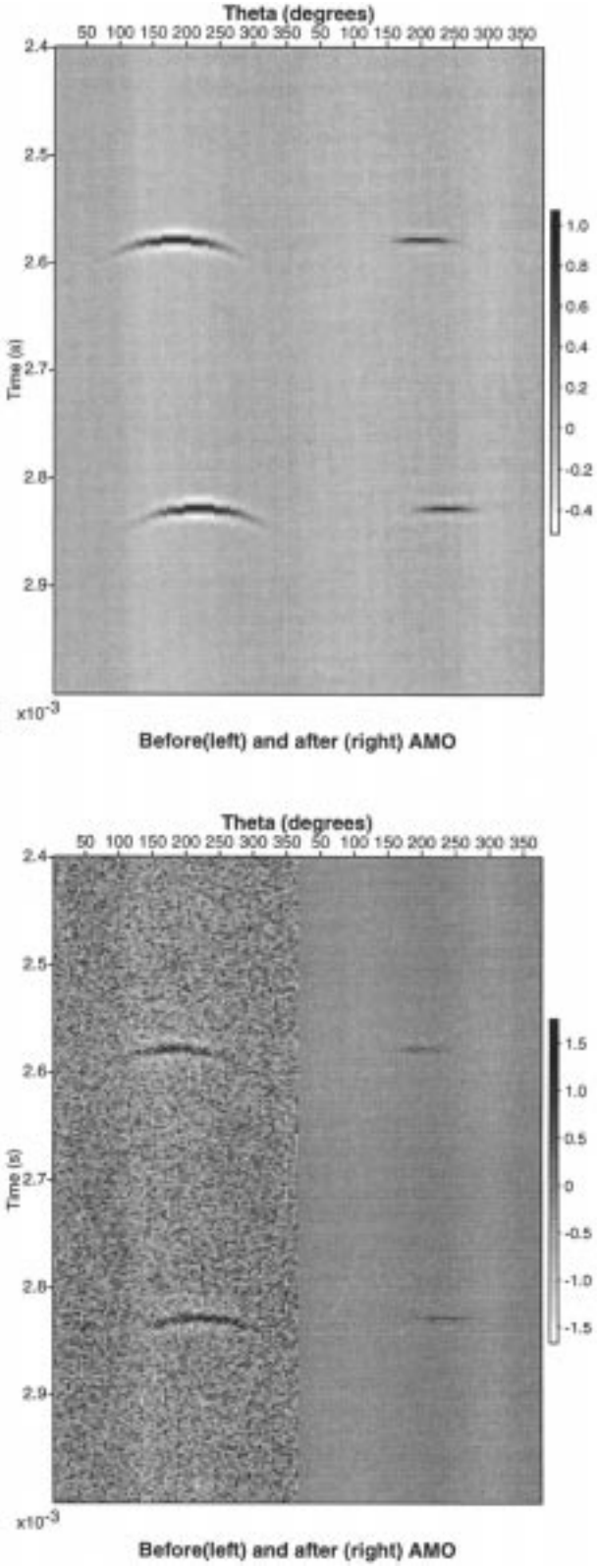

Fig. 11. Synthetic examples for two scattering points before AMO (left side) and after AMO (right side), without noise(top), and with noise (bottom). The energy is again focused in both cases. We obtain a good improvement of the method even in the presence of a high level of noise.

Notice that, even with the high level of noise, we can recover the acoustic signature of the two scatterers and localize them.

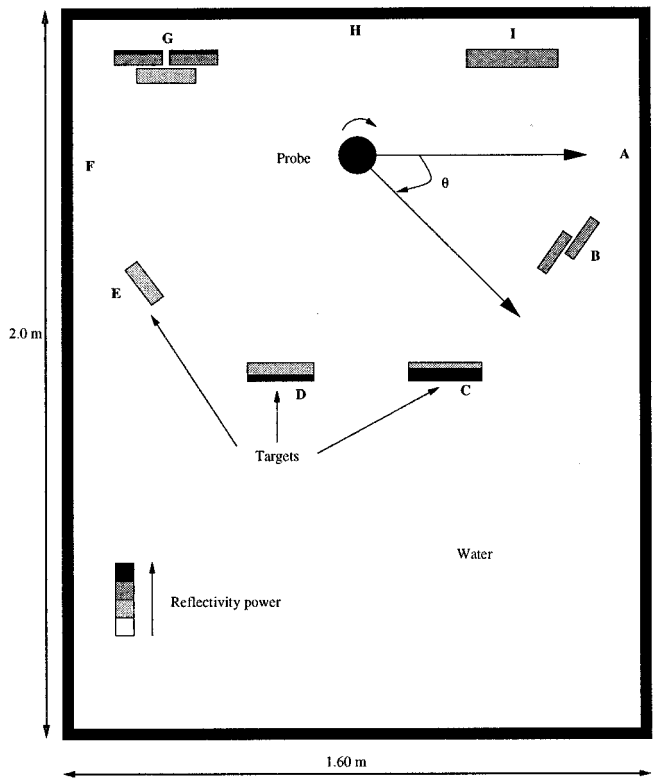

Fig. 12. Top view of the water tank experiment for testing the AMO focusing algorithm.

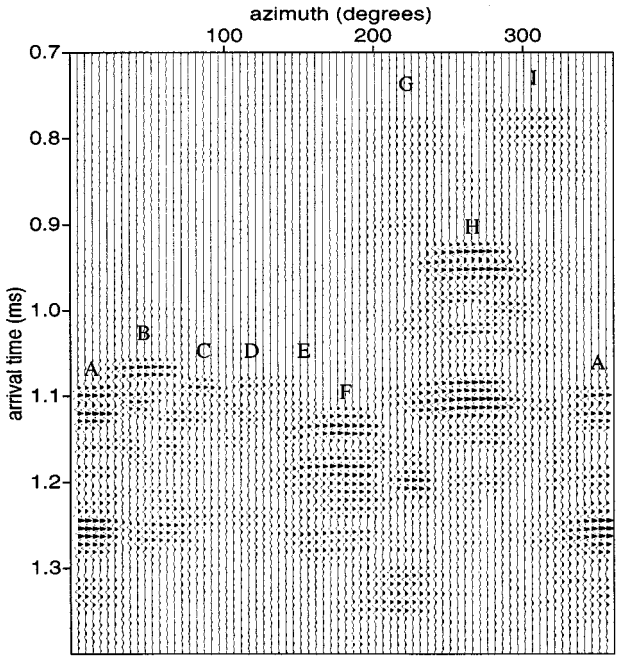

Fig. 13. Data corresponding to the experiment shown in Fig. 12 and obtained by operating the endoscopic probe at single depth and offset.

These preliminary tests on synthetic examples show the reliability of this method.

IV. Laboratory Acoustic Experiments

In the following, we present experiments performed in a water tank (dimensions 2.0 m $\times$ 1.6 m $\times$ 1.5 m) to illustrate the azimuthal imaging capabilities of the probe, and to test the preprocessing AMO algorithm discussed in the previous section. For each experiment, 72 traces per common offset gather are measured by the receiver cell or "ear" (pair of hydrophones) which correspond to an acquisition every five degrees. These responses are sampled synchronously ($fe = 500$ kHz) and recorded by the analog-to-digital (A/D) converter (2048 samples per trace). The numerical signals are then transferred to the computer to be treated. One complete acquisition ($0 < \theta < 360°$) takes *less than 2 min*. The source signal issued from the numerical generator is a Ricker function in time (second-order derivative of a Gaussian function). It is then amplified before it is sent to the hydrophone-source. All these experiments are automatized and controlled by the computer. The software development was done using Labview [22].

A. Experiment in the Presence of Different Scatterers

The first experiment was done in open water (i.e., without a borehole) to assess the azimuthal directivity when the record data (seismic traces) are not perturbed by strong borehole modes ([8], [23]–[25]). The design of this experiment is shown in Fig. 12. Reflectors with different impedance contrast and reflectivity characteristics, presenting different shape and thickness (Plexiglas bodies combined with different absorbing materials) are placed around the probe, at different distances. These reflectors are vertical and span the whole water depth in the tank, so they may safely be considered in a 2-D geometry (i.e., not varying with respect to depth z). The data were acquired at a single depth and offset. The probe rotates vertically, while its isotropic source emits a Ricker waveform with central frequency of 100 kHz whose echoes are detected by the receiver cell pointing toward the azimuthal direction θ. The data obtained consist in time-series corresponding to different azimuths by step $\delta\theta = 5°$.

Results: The recorded data are shown in Fig. 13, where the echoes corresponding to both the targets and walls of the tank located around the probe are clearly visible. However, the signals associated with nearby targets, like those located at an azimuth of 90°, strongly overlap. This results in a blurring of the image which can be partly corrected with the AMO processing. The application of the AMO algorithm to these experimental data is shown in Fig. 14. As expected, the focusing is limited by the visibility angle ($\alpha = 45°$) of the window in the absorbing cylinder since the arrival times are identical in this angular region. This AMO correction proved its efficiency as can be observed on real data set.

B. Experiment in the Presence of a Miniature Concrete Borehole, Without Scatterers

A second series of experiments was done with a concrete pipe simulating the effects of a borehole to account for the presence of strong borehole waves as in real field experiments [26], [27]. Of course, this experiment is not identical to real conditions where behind the borehole we have formation rock. Our interest in this case is to show the use of the AMO algorithm to remove the influence of these tube waves. In real conditions, the only important issue is the penetration of the input signal into the

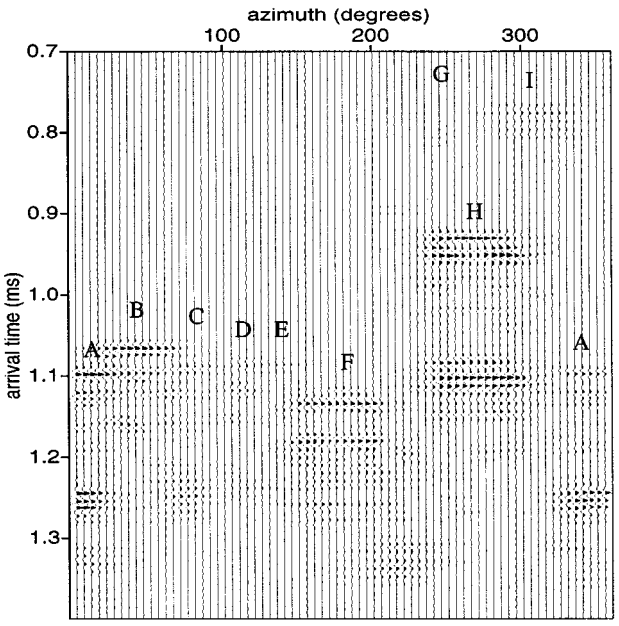

Fig. 14. Data of Fig. 13 corrected with the AMO algorithm.

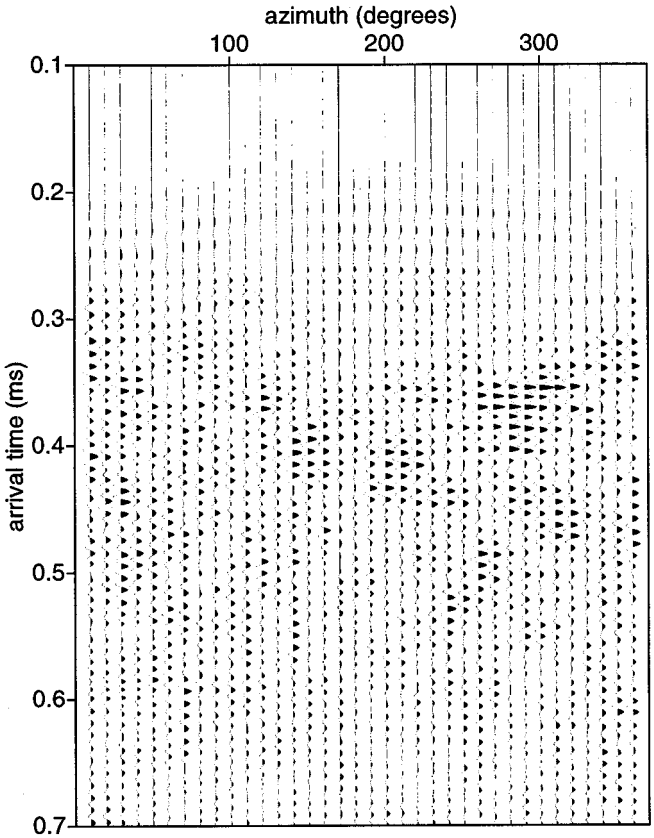

Fig. 15. Data of the experiment made with a concrete pipe simulating a borehole. Strong borehole waves with wiggly arrival times are visible on the whole azimuthal range.

formation, which is strongly dependent of the frequency of the source signal. First, we studied the effect of tube waves generated by a cement pipe built in the laboratory, without scatterers, put in the acoustic tank. The scattering effect in this experiment is only due to the walls of the tank. The data recorded, for a fix offset and depth, are shown in Fig. 15 where strong borehole

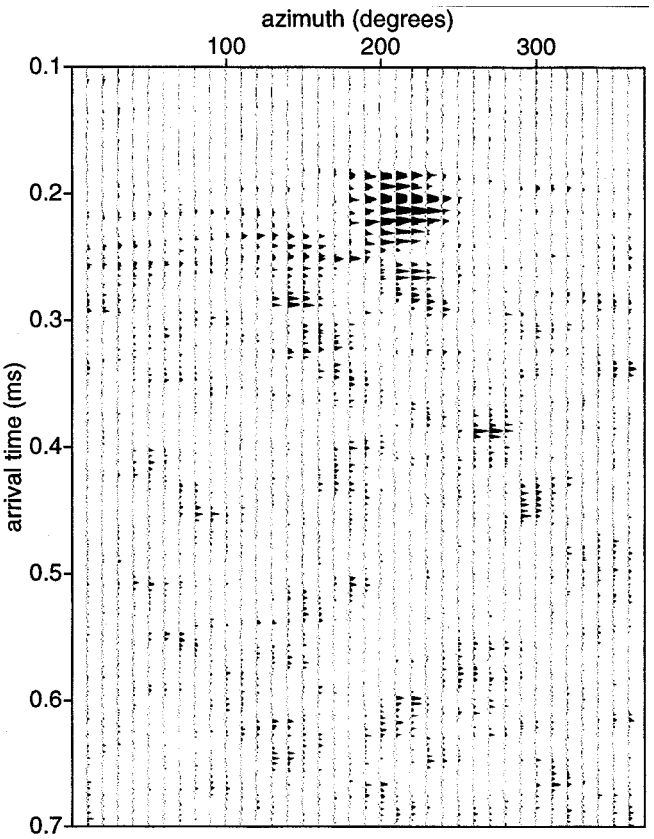

Fig. 16. AMO-corrected data of Fig. 15. Most borehole waves have been destroyed while an early arrival located around $\theta = 200°$ and not very apparent in the original data has been sharply enhanced.

waves can be seen. These waves propagate along the borehole boundary and in either the water or the mud filling the borehole. Since the source is isotropic, the borehole waves are excited in an azimuthal-invariant way and they appear continuous on the whole azimuthal range, contrary to the echoes coming from the targets in the first experiment and which are visible in a limited azimuthal range (see Fig. 13). In principle, variations of the arrival times with respect to the azimuth could also be due to longitudinal inhomogeneities of the sound velocity in the pipe. Such inhomogeneities are however unlikely to be both sufficiently strong and of a large extent to produce important deviations in the arrival times. Indeed, we have never unambiguously observed such effects.

Result—Filtering Tube Waves With AMO: In the previous section, the efficiency of the AMO method to focus the correct recorded data from the directivity function of the receivers was clearly demonstrated. Nevertheless, in real conditions, we need to consider the strong tube waves which mask weak reflections coming far from the borehole. The AMO algorithm can also be used to filter the borehole waves while preserving early reflections coming from targets, as shown in Fig. 16. For the present instance, the AMO algorithm is applied to a trace attribute different from the previous example. Most borehole waves are destroyed while a strong wave packet located around $\theta = 200°$, not very apparent in the original data, is enhanced. This is due to a local deformation of the pipe, accentuated by the position of the probe which is not centered in the borehole. Outside the pipe, the AMO algorithm allows us to detect the reflections on

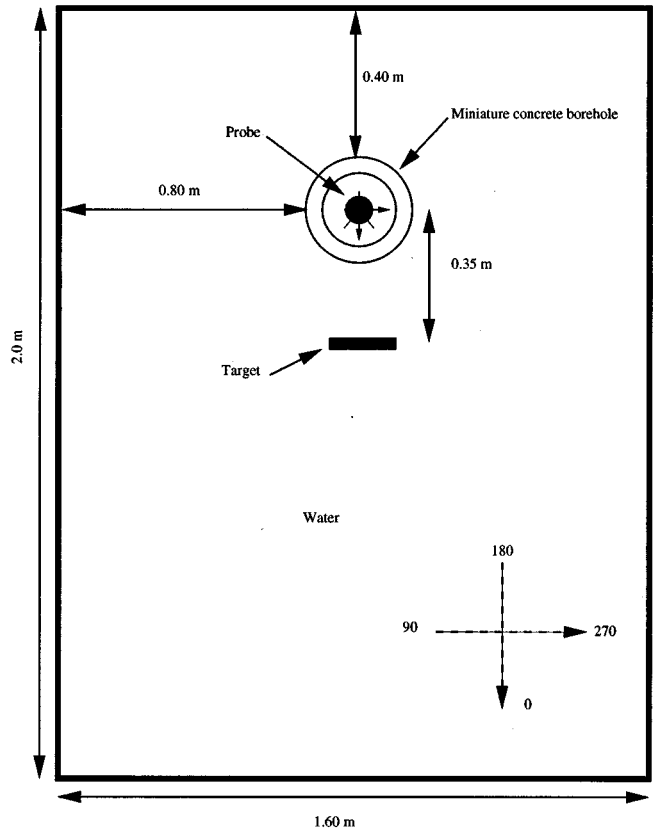

Fig. 17. Design of the second experiment. A metallic plate is put at a distance of 0.35 m from the probe. An acquisition is made for a common offset and depth versus azimuth.

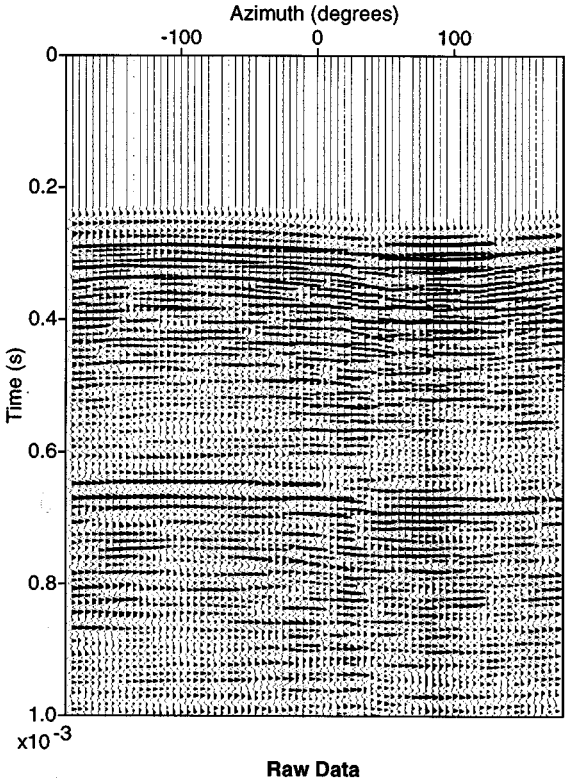

Fig. 18. Initial experimental data recorded in acoustic tank the probe being in the concrete borehole. We notice that it is impossible to detect echoes corresponding to the metallic plate. The object is centered around the azimuth 0°, and should be localize around the time 0.54 ms.

the walls tank (weak scatterers) among the ambient noise (e.g., around the time $t = 0.20$ ms for $\theta = 130°$ and $\theta = 220°$, then $\theta = 260°$ for the time $t = 0.39$ ms).

V. Complete Experiment: Filtering Borehole Waves in Presence of Scatterer Using Continuous Wavelet Transform and AMO Algorithm

A metallic plate located at a distance $d = 0.35$ m from the probe, at the azimuth 0° outside a concrete miniature borehole used in civil engineering is now introduced into a water tank (see Fig. 17). The corresponding recorded data are shown in Fig. 18. The signature of the object (scattering response) is masked by strong borehole waves generated in the same spectral range as the waves generated by the object. The sinusoidal-like shape of the wavetrains can be explained by the fact that the probe was not precisely centered into the borehole, and the variations in the amplitude are due to the inhomogeneities of the pipe. In particular, the strong amplitude around $\theta = 90°$ corresponds to a longitudinal junction in the concrete forming the pipe. This strong reflection proves the efficiency of the directive probe that allows to detect precisely the position of the junction (similar to a fracture) in the azimuthal domain. However, the difficulty consists here in extracting the weak reflections of the metallic plate from the recorded azimuthal section where they interfere with the borehole waves reinforced by the effect of the cement junction. The use of a time-scale method as the continuous wavelet transform becomes necessary to detect and extract from real data the signature of the objects, fractures, or abrupt changes [28] hidden from borehole waves.

This transformation applied to an arbitrary signal provides simultaneously a spread of its energy in the time-frequency plane or time-scale half-plane $(b,\, a)$. More precisely, the continuous wavelet transform of a signal $s(t)$ is the scalar product of this signal with a family of elementary functions g called wavelets dilated in time by the scale factor a and translated in time by the factor b such as $T^b D^a[g(t)] = (1/a)g[(t-b)/a]$. The general equation of this transformation is written as follows:

$$S(b,\, a) = \frac{1}{a} \int s(t) \overline{g} \left(\frac{t-b}{a} \right) dt \tag{3}$$

where $\overline{g}$ is the complex conjugate of g.

The small dilatation parameters are related to the high frequencies and reverse, while the translation parameter is homogeneous to the time. The choice of the analyzing wavelet is free. Here, we used a Morlet wavelet. We imposed it to be progressive (i.e.: $\hat{g}(\omega) = 0$, $\omega < 0$), that is, a necessary condition to define correctly the phase of the wavelet coefficients with a physical meaning. The phase and the spectral components of different waves can be precisely calculated without artifact (interferences due to the Fourier components on the negative axis) [28]. If the

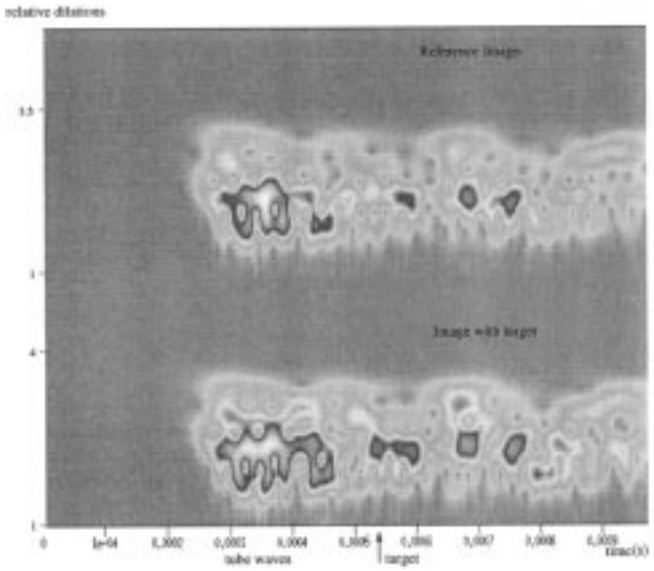

Fig. 19. Modulus of the wavelet transform of seismic trace recorded with object (bottom), and without object (top: reference imaging) for a fixed θ and z position. We can easily see the presence of different waves packets arriving at different times, and corresponding to different spectral range. The localization of the echo linked to the presence of metallic plate is seen at the arrival time 0.54 ms, whereas the first waves packets are generated by the borehole in same frequency range that the weak useful signal.

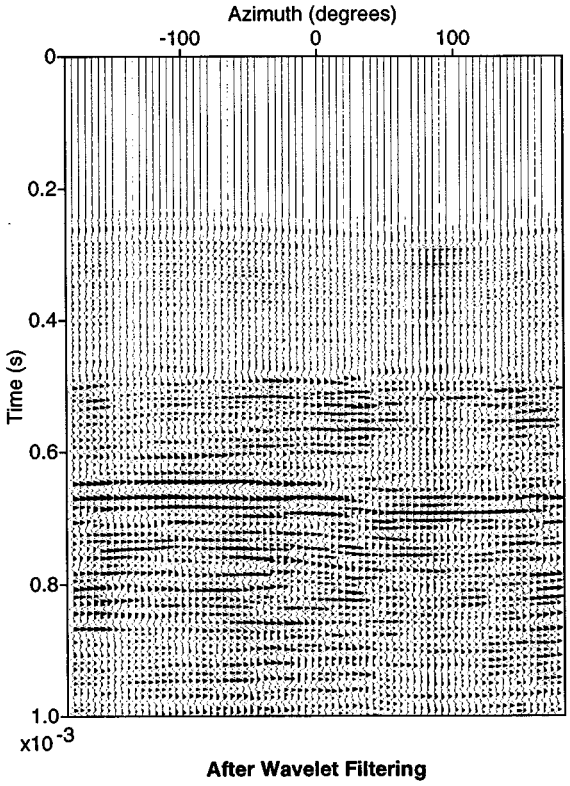

Fig. 20. Experimental data (see Fig. 18), after wavelet filtering. The tube waves are filtered. Only a weak signal, not taking into account our filtering, is present. It corresponds to the borehole junction around the azimuth 100.

wavelet function respects the admissibility condition, an inversion formula therefore exists that allows us to reconstruct the signal

$$s(t) = \Re\left[c_g^{-1}\int S(b,\,a)a^{-1}g\left(\frac{t-b}{a}\right)\,\frac{da\,db}{a}\right] \qquad (4)$$

where $\Re$ corresponds to the real part of the equation and c_g a constant related to the admissibility condition defined as

$$c_g = 2\pi\int\frac{|\hat{g}(\omega)|^2}{\omega}\,d\omega. \qquad (5)$$

This means $\hat{g}(0) = 0$, where $\hat{g}$ is the Fourier transform of g.

The reader can refer to [29] for more information about the continuous wavelet transform and its applications.

The filtering of the borehole waves is made using the technique developed in [19]. Because of the symmetry properties of the concrete pipe along the depth, we have an invariance of the acoustic signature of the tube waves. We can select a specific polygon in the half-plane $(b,\,a)$ corresponding to this signature, whatever the depth z. A wavelet reconstruction formula can then be applied to build the analytic signal corresponding to the selected time-frequency domain. Knowing this analytic signal, it is easy to filter it from the initial data.

Results: Fig. 19 presents the wavelet transform of two tracks recorded by the probe with and without the presence of an object in the acoustic tank. These traces correspond to two different experiments done in the presence and absence of the metallic plate. Independently of the signature of the tube waves, the object is clearly observed on this representation (bottom) around the arrival time 0.54 ms where first wave packet corresponds to the borehole waves. The wavelet coefficient of the reference imaging (seismic trace without object) is shown at the top. The azimuthal θ and depth z are fixed, and the wavelet transform is performed on the time variable. The time-frequency domain corresponding to the borehole waves is selected from the analysis of different acquisitions with respect to the azimuth. For each depth, the azimuthal symmetry of the borehole waves is used. In other words, all these waves are concentrated in the same time-frequency domain independently of the azimuth, because they are due only to the cylindrical concrete borehole. Therefore, they play the role of an acoustic signature of the tube.

The reconstruction formula allows us to build the analytic signal of these waves, so we can subtract these reconstructed borehole modes from the initial data. Fig. 20 shows the result of the wavelet filtering for the recorded section. The borehole waves are filtered but the signature of the borehole junction is always visible on the section with a smallest amplitude. This is due because we have not locally taking the effect of this perturbation into account. The AMO algorithm is then applied to focus the information as presented previously (Fig. 21). The object is now clearly detected on the recorded data around the time $t = 0.54$ ms as expected.

VI. Conclusion

Quick 3-D imaging from boreholes is an increasing necessity in many situations encountered in civil engineering and environmental studies. In the present paper, we have presented a simple borehole probe, designed with standard devices, which enables 3-D cylindrical imaging. The produced images can be

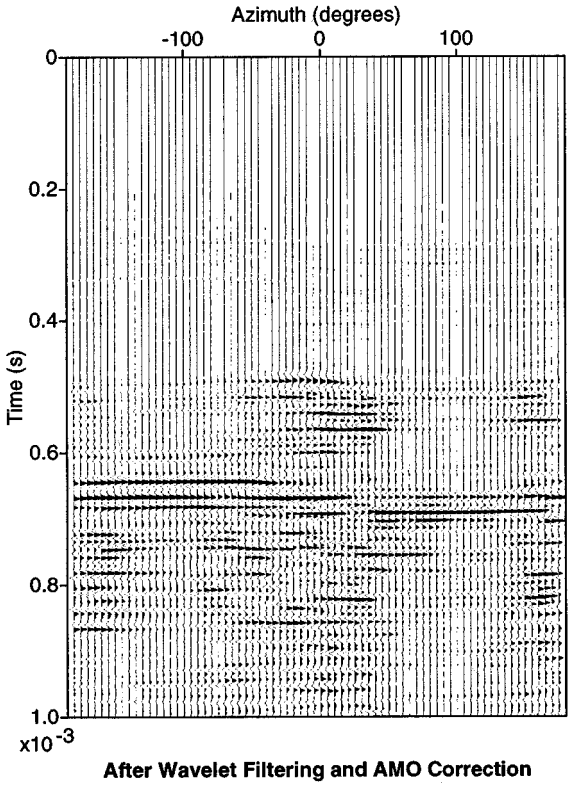

Fig. 21. Experimental data after wavelet filtering and AMO corrected. The acoustic signature of the object present out of the borehole is detected as expected at the time 0.54 ms, around the azimuth 0.

further processed through the AMO algorithm to both sharpen a deblurring of some overlapping echoes and filter out strong borehole waves. The azimuthal DOF provided by the probe offers a new way to process seismic data and, in particular, to discriminate among various type of waves like reflections or tube waves, as shown in Section IV-A. Current acquisition methods in boreholes do not consider this point. In addition, the directive condition on the recorded data allows us to obtain an accurate detection of heterogeneities around the borehole (e.g., fractures, specific cavities). This sort of information is moreover an important challenge for reservoir engineering, nondestructive testing in environmental problems where a good knowledge of location of fractures in geological structure is primordial. In a more general case (see Section V) when tube waves and local surface waves (defect of the pipe) mask the reflections coming from thin targets, (fracture, interface, or a texture variation in a thin layer), time-scale filtering combined with AMO algorithm allow us to remove them and localize the object in the azimuthal section.

The basic imaging algorithm of the endoscopy method presented in this paper can be the following: filtering the borehole modes and focusing the information in the azimuthal domain.

- The first step consists in selecting the data in the (θ, t) domain.
- For each section, a wavelet filtering of borehole waves is carried out, then a correct focusing of data energy is performed by the AMO correction.
- The data are then spread in (Z, t) sections, where it is possible to apply a migration for each section.

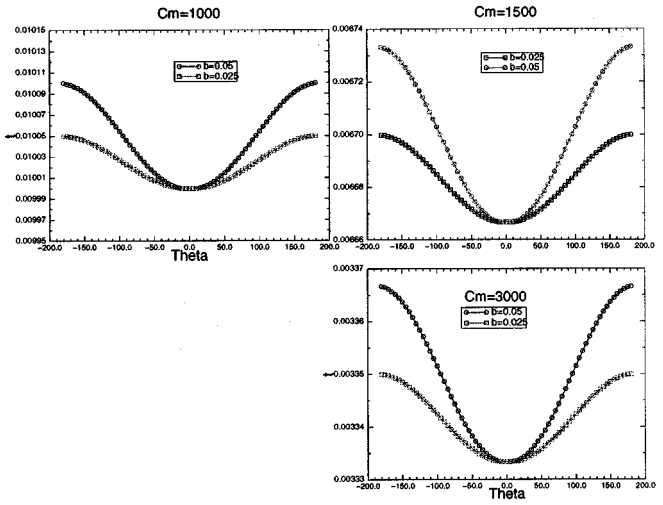

Fig. 22. Behavior of AMO function for different velocities and "ear" radius. The larger the "ear" the more important the focusing effect. It is interesting to remark that the velocity variation does not take place on the shape curves. These different curves are shifted in time in order to be compared.

A cylindrical image is obtained which provides a 3-D azimuthal imaging around the borehole.

Appendix
Sensitivity of the AMO Method

In this Appendix, the influence of the parameters on the AMO equation is studied. One parameter will be fixed and the AMO equation will be studied as a function of azimuth. All of the tests are done with azimuth angles enclosed in the interval $[-\pi, \pi]$ to be consistent with the characteristics of the probe previously presented. Equation (1) is rewritten considering geological situation

$$t(B, D, \theta, \alpha, c_m, c_r) = \frac{1}{c_r} \times \left[\frac{B}{c_m} + \sqrt{\frac{B^2}{c_m^2} + \frac{D^2}{c_m^2} - \frac{2BD}{c_m^2} \cos\left(|\delta\theta| - \frac{\alpha}{2}\right)} \right]$$

with the radius b of the borehole such that $B = b.c_r$, the distance d between the scatterer and the probe $D = d.c_m$, where c_r is an AMO velocity which depends on the velocity in the surrounding rocks (see Section III-A) and c_m the velocity of the borehole mud. The study is done with respect to the variation of the ratio of these velocities.

We first consider the AMO function when the distance of the probe is fixed during all the experiment.

1) $c_m = c_{m_o} = cte, D = D_o = cte$: The behavior of the AMO function is now evaluated when the radius of the directional receiver varies. The AMO function is sharpest if the radius of the directional element increases, means the focusing effect will be most important. This remark is important for the design of the tool. The ideal case will be to take a radius closest to the borehole radius size to increase the focusing property of the directional receiver. Fig. 22 shows the variation of the AMO function for a fix receiver radius size and various speed and distance.

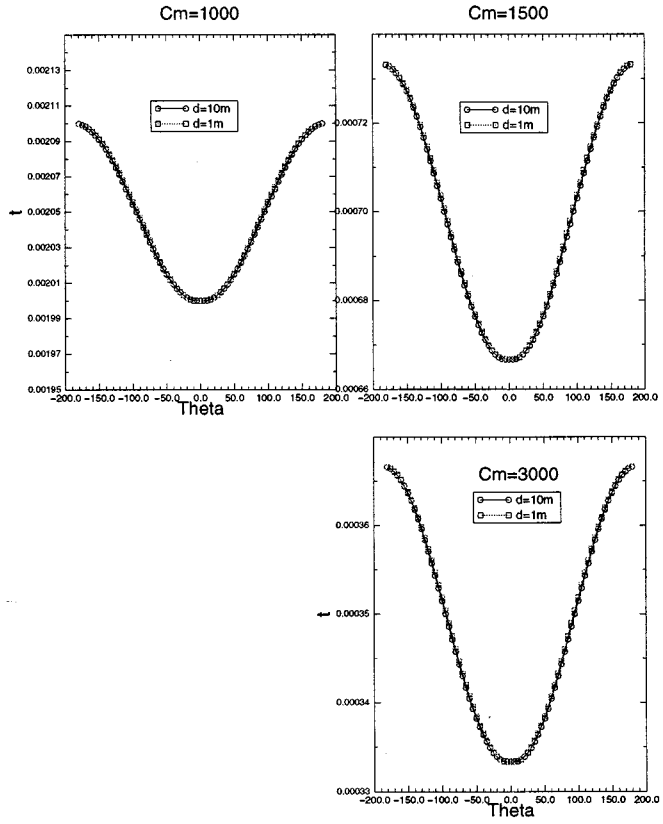

Fig. 23. Variation of AMO function for different velocities and different distances for a fixed "ear" radius. We note that neither the velocity nor the distance influence in a significant way the shape of AMO function. These curves have been shifted in time to order to be compared.

2) $c_m = c_{m_o} = cte, B = B_o = cte$*:* This case corresponds to the behavior of the AMO function as a function of the distance probe-scattering point, when the velocity varies. As expected, only the travel time is dependent of the distance. A variation of the distance scattering-point probe for different velocities will not influence the behavior of the angular directivity. We have obtained results comparable (Fig. 23). These two parameters do not play a dominating role.

The estimated speed c_r on the AMO correction is the most important parameter of the method. Its value can greatly influence the quality of the processing on real data. The importance of the design of the directive receiver to improve the quality of the AMO processing has also been demonstrated.

ACKNOWLEDGMENT

The authors want to thank M. LeMoine for his help and collaboration in the development of the probe. They also thank Y. Guéguen, J. Lancelot, and P. Lebon for their strong support since the beginning of this project, the CNRS-INSU Geomechanique Desreches Profundes (GDR), and the GDR FORPRO.

REFERENCES

[1] J. L. Avis and A. P. Annan, "Ground penetrating radar for high-resolution mapping of soil and rock stratigraphy," *Geophys. Prospecting*, vol. 37, pp. 531–551, 1989.

[2] H. R. Burger, *Exploration Geophysics of the Shallow Subsurface*. Englewood Cliffs, NJ: Prentice-Hall, 1992.

[3] E. L. Hardin, C. H. Cheng, F. L. Paillet, and J. D. Mendelson, "Fracture characterization by means of attenuation and generation of tube waves in fractured crystalline rock at mirror lake, New Hampshire," *J. Geophys. Res.*, vol. 92, no. B8, 1987.

[4] D. C. Nobes, "Troubled waters: Environmental applications of electrical and electromagnetic methods," *Surv. Geophys.*, vol. 17, pp. 393–454, 1996.

[5] W. E. Kelly and S. Mares, *Applied Geophysics in Hydrogeological and Engineering Practice*. New York: Elsevier, 1993, vol. 44.

[6] C. H. Cheng, N. M. Toksoz, and M. E. Willis, "Determination of in situ attenuation from full waveform acoustic logs," *J. Geophys. Res.*, vol. 87, no. B7, pp. 5477–5484, 1982.

[7] E. Fisher, "Acquisition and processing of wide-aperture ground penetrating radar data," *Geophysics*, vol. 57, no. 3, pp. 495–504, 1992.

[8] F. L. Paillet and C. H. Cheng, *Acoustic Waves in Borehole*. Boca Raton, FL: CRC, 1991.

[9] B. A. Hardage, *Vertical Seismic Profiling, A: Profiling, Geophysical Exploration*, Helbig and Treitel, Eds: Geophysical Press, 1983.

[10] M. Oristaglio, "A guide to current uses of vertical seismic profiles," *Geophysics*, vol. 50, pp. 2473–2479, 1985.

[11] C. V. Kimball and T. L. Marzetta, "Semblance processing of borehole acoustic data," *Geophysics*, vol. 49, pp. 530–544, 1987.

[12] B. E. Hornby, "Imaging of near-borehole structure using full-waveform sonic data," *Geophysics*, vol. 54, no. 6, pp. 747–757, 1989.

[13] C. Esmersoy, "Inversion of P and SV waves from multi-component offset vertical seismic profiles," *Geophysics*, vol. 55, pp. 39–50, 1990.

[14] J. Zemanek, E. E. Glenn, L. J. Norton, and R. L. Caldwell, "Formation evaluation by inspection with the borehole televiewer," *Geophysics*, vol. 35, no. 2, pp. 254–269, 1970.

[15] F. L. Paillet and J. E. White, "Acoustic modes of propagation in the borehole and their relationship to rock properties," *Geophysics*, vol. 47, no. 8, pp. 1215–1228, 1984.

[16] W. M. Telford, L. P. Geldrat, R. E. Sheriff, and D. A. Keys, *Applied Geophysics*. Cambridge, U.K.: Cambridge Univ. Press, 1985.

[17] D. Miller, M. Oristaglio, and G. Beylkin, "A new slant on seismic imaging: Migration and integral geometry," *Geophysics*, vol. 52, no. 7, pp. 943–964, 1987.

[18] G. Salvini, "Image temps-réel par traitement d'antenne hybride: Application," Ph.D. dissertation, Univ. St. Jerôme, Univ. III, Marseille, France, 1985.

[19] H. P. Valero, "Seismic endoscopy," Ph.D. dissertation, Geophysics, Mise au point d'une méthode d'endoscopie sismique 3-D en géophysique de puits: Développements and traitement de l'information, IPG-Paris, CNRS-UPR 4661 Campus de Beaulieu, Rennes, France, 1997.

[20] J. A. Scales, *Theory of Seismic Imaging*. Berlin, Germany: Springer-Verlag, 1995.

[21] D. Kahaner, C. Moler, and S. Nash, *Numerical Methods and Software*. Englewood Cliffs, NJ: Prentice-Hall, 1988.

[22] G. W. Johnson and Labview Graphical Programming, *Practical Applications in Instrumentation and Control*. New York: McGraw-Hill, 1994.

[23] M. A. Biot, "Propagation of elastic waves in a cylindrical bore containing a fluid," *J. Appl. Phys.*, vol. 23, no. 9, pp. 997–1005, 1952.

[24] M. A. Biot, "Theory of propagation of elastic waves in a fluid saturated porous solid: Low frequency range," *J. Appl. Phys.*, vol. 28, no. 2, pp. 168–178, 1956.

[25] M. A. Biot, "Theory of propagation of elastic waves in a fluid saturated porous solid: High frequency range," *J. Appl. Phys.*, vol. 28, no. 2, pp. 179–191, 1956.

[26] K. M. Tubman, C. H. Cheng, and N. M. Toksoz, "Synthetic full waveform acoustic logs in cased boreholes," *Geophysics*, vol. 49, no. 7, pp. 1052–1059, 1984.

[27] K. W. Winkler, H.-L. Liu, and D. L. Johnson, "Permeability and borehole stoneley waves: Comparison between experiment and theory," *Geophysics*, vol. 54, no. 1, pp. 66–75, 1989.

[28] G. Saracco, "Propagation of transient waves through a stratified fluid medium: Wavelet analysis of a nonasymptotic decomposition of the propagator," *J. Acoust. Soc. Amer.*, vol. 95, no. 3, pp. 1191–1205, 1994.

[29] A. Grossmann and J. Morlet, "Decomposition of Hardy functions into square integrable wavelets of constant shape," *SIAM J. Math. Anal.*, vol. 15, pp. 723–736, 1984.